



# Effect of molar concentration on structural, magnetic domain and optical properties of BiFeO<sub>3</sub> thin films

R. R. Awasthi<sup>1</sup> · K. Asokan<sup>2</sup> · B. Das<sup>1</sup>

Received: 11 December 2018 / Accepted: 15 March 2019 / Published online: 19 April 2019  
© Springer-Verlag GmbH Germany, part of Springer Nature 2019

## Abstract

Pure crystalline bismuth ferrite BiFeO<sub>3</sub> (BFO) thin films have been deposited on the cleaned glass substrate by sol–gel spin-coating technique with different molar concentrations (from 0.1 to 0.5 M) of the precursor solution. The influence of molar concentrations on the structural, magnetic and optical properties has been investigated by different advanced techniques. The X-ray diffraction patterns of BFO films revealed that the increase of the molar concentration from 0.1 to 0.5 M induced the structural transformation from distorted orthorhombic to single orthorhombic phase. The average crystallite size of BFO thin films was calculated using Scherrer formula and found to be in the range of 15–28 nm. The elemental composition of Bi, Fe and O was confirmed using energy-dispersive spectroscopy of X-rays. The atomic force microscopic images revealed that shape of particles are changing from ellipsoid to nanorods with increasing the molar concentration from 0.3 to 0.5 M. The root means square roughness of BFO films was also varying from 6.34 to 29.88 nm. The stripe-like structure of domain was explored through magnetic force microscopy. The films prepared from the precursor of molar concentration of 0.5 M revealed the microscopic remnant magnetization of 0.19 emu/cm<sup>3</sup> and coercivity of 443.06 Oe from the *M–H* measurements. This enhancement of ferromagnetic properties may be due to the formation of nanorods resulted by destroying the cycloid spin structure. The optical bandgaps were also tuned from 2.58 to 2.49 eV due to increase of the crystallite size from 15 to 28 nm.

## 1 Introduction

During the last few decades, multiferroic thin films have attracted enormous significant interest in the material science research because it simultaneously exhibits ferroelectric and antiferromagnetic properties in the same phase as well as strong coupling between the charge and spin ordering at room temperature [1–3]. The most interesting properties of multiferroic materials are magnetoelectric (ME) effect in which the electric polarization can be tuned by the application of magnetic field and magnetization can be tuned by the application of electric field [4–6]. The bismuth ferrite (BiFeO<sub>3</sub>), being a single-phase material, shows linear magnetoelectric effect [7–10] at room temperature. It is the most suitable materials for various applications in spintronics, microelectronics, magnetic field sensors and multiple-state

memories devices [11–13] due to its high Curie temperature  $T_C \sim 1103$  K and low Neel temperature  $T_N \sim 643$  K [14]. Besides, there is another class of hexaferrite materials BaFe<sub>12–x</sub>Al<sub>x</sub>O<sub>19</sub> that are also promising for practical use [15–17]. However, good ferromagnetic nature, i.e. large total magnetic moment at operating temperature (room temperature) is also very important. Substituted M-type hexaferrites [18–20] are excellent candidate for such magnetic material with  $T_C \sim 740$  K. This is the simplest type of all ferrites with a hexagonal structure. More than 90% of permanent magnets are produced all over the world based on this compound. This compound is a deep semiconductor ( $\rho \sim 10^9$  Ohm cm) at room temperature with a ferrimagnetic structure and a total magnetic moment of  $20 \mu_B$  in the ground state. The single-phase BFO thin film exhibits both the rhombohedral/hexagonal or pseudo-cubic structure with R3c space group, where the pseudo-cubic [111]<sub>C</sub> is equivalent to hexagonal [001]<sub>h</sub> direction. The covalent interaction originates from the strong hybridization between Fe-3d orbital and O-2p orbital. It causes the tilt of FeO<sub>6</sub> octahedra. This tilt of octahedra plays a significant role in the structural distortion of the BFO lattice. The shifting of the atoms and rotation of FeO<sub>6</sub> octahedra allow the induced polarization that may be

✉ B. Das  
bdas2260102@gmail.com

<sup>1</sup> Department of Physics, University of Lucknow,  
Lucknow 226007, India

<sup>2</sup> Inter-University Accelerator Centre, New Delhi 110067,  
India

related to the lattice strain. The magnetic studies revealed that BFO has a G-type antiferromagnetic structure with a small rotating helical magnetic ordering period of rotation  $\sim 62$  nm [21, 22]. The R3c symmetry also permits a canting of the antiferromagnetic sublattice, resulting in a weak ferromagnetism, if the magnetic moment of  $\text{Fe}^{3+}$  is oriented perpendicular to the [001] direction [11, 23]. Moreover, as previously reported, the ferromagnetic properties of BFO materials are increasing with decreasing particle size, due to the increase of surface to volume ratio [24–26]. Whereas the recent theoretical studies using first-principle density functional theory also confirmed the existence of a large ferroelectric polarization as well as a small magnetization in the BFO thin films [27]. Furthermore, large spontaneous polarization and multiferroic properties at room temperature have been recently discovered in barium hexaferrites substituted by diamagnetic cations. Herewith the magnetoelectric characteristics of M-type hexaferrites fabricated by a modified ceramic technique are more advanced than those for the well-known room temperature  $\text{BiFeO}_3$  orthoferrite multiferroic [28–31]. The bismuth ferrite thin films have the limit for technological application due to its high leakage current density originated possibly from Bi-deficiency, (high volatility of Bi), oxygen vacancy and charge fluctuation of ( $\text{Fe}^{3+}/\text{Fe}^{2+}$ ) ions. To suppress the leakage current density and to improve weak ferromagnetism, many attempts have been made such as modifying the surface properties, for example, thickness [32, 33] and morphology [34–36] at the nanoscale, high magnetic field annealing [37–39] and doping of various metal ions [40–55]. Since the synthesis of single-phase BFO is very difficult due to high volatility of Bi, the researchers have used various other techniques, for example, spray pyrolysis [56], sol–gel spin coating [57], pulsed laser deposition [58], and metal organic deposition [59] for the preparation of single-phase BFO thin films. However, the substitution of strong ferromagnetic compounds by diamagnetic cations [19] has also been adopted for synthesizing single-phase materials. Besides, for the modification of surface structure and multiferroic properties, the films were deposited on different substrates such as Pt/TiO<sub>2</sub>/SiO<sub>2</sub>/Si/SrTiO<sub>3</sub> [60–65]. There are still few reports [66, 67] on the synthesis of  $\text{BiFeO}_3$  thin films by spin-coating method with varying molar concentrations of precursor solution. In view of the above facts, sol–gel spin-coating technique, because of lower deposition temperature, precise control of composition and thickness, high purity, and better chemical homogeneity over large area, is employed for single-phase BFO thin film preparation from varying molar concentrations (0.1–0.5 M) of precursor solution in the present investigation. This method also influences the surface morphology and grain/crystallite size distribution and hence it significantly enhances the multiferroic properties [68–78]. The effect of molar concentrations of the precursor solution on

the crystal structure, surface morphology, optical and magnetic properties of  $\text{BiFeO}_3$  thin films is herewith reported.

## 2 Experimental details

The BFO thin films have been deposited on cleaned glass substrate by sol–gel spin-coating technique at room temperature. The analytic grade materials of bismuth nitrate [ $\text{Bi}(\text{NO}_3)_3 \cdot 5\text{H}_2\text{O}$ ] and iron nitrate [ $\text{Fe}(\text{NO}_3)_3 \cdot 9\text{H}_2\text{O}$ ] have been used for the preparation of precursor solutions. To prepare precursor solutions of 0.1 M, 0.485 gm of bismuth nitrate pentahydrate and 0.404 gm of iron nitrate were dissolved in 20 ml solution (18 ml of 2-methoxy ethanol + 2 ml of acetic acid) and stirred continuously for 2 h. The acetic acid acts as a chelating agent and stabilizes the gel solution. Thereafter prepared precursor solutions of 0.1 M were again undergone for constant stirring at 70 °C for 1 h to get the homogeneous and transparent brownish colour solution. Further, for getting the viscous solution, resultant sol was aged at room temperature for 24 h. Similarly, the molar concentration of precursor solution was tuned to 0.3 M and 0.5 M. Before deposition, the substrates were cleaned by organic solvent such as acetone, isopropyl alcohol and distilled water to remove any dust or contaminants present on the surface of the glass slides. Finally, BFO thin films have been deposited with different molar concentration of precursor solution by spin-coating technique at 3500 rpm for 30 s. After each deposition, the film was heated to 350 °C for 30 min to decompose and evaporate the organic compounds present in the films. The deposition process was repeated 15 times to obtain appropriate and desired thickness of the films. Finally, the prepared thin films with different molar concentrations of precursor solution were annealed at 500 °C for 4 h in an open-air atmosphere for crystallization. The gross structure and chemical phase purity of BFO thin films were examined by powder X-ray diffractometer (PXRD) [Rigaku, Ultima-IV] with  $\text{CuK}\alpha$  radiation ( $\lambda = 1.5406$  Å). The PXRD data were collected for scanning range of  $2\theta$  from 20°–60° under scanning speed of 0.5°/min and a step size of 0.02°. The surface morphology and chemical composition of the films were explored through field emission scanning electron microscope (FE-SEM) of MIRA II LMH from TESCAN attached with energy-dispersive X-ray spectroscopy (EDS) detector. Before getting the SEM micrographs, thin films were coated with gold film of 10 nm thickness in a high-vacuum turbo pumped sputter coating system. The surface topography as well as root mean square (RMS) roughness of BFO films were examined by atomic force microscopy. The maximum scan area for getting the images was  $10 \times 10 \mu\text{m}^2$ . The magnetic phase images were also recorded by magnetic force microscopy (MFM) with the multimode SPM (Digital Instrument Nanoscope E) at

room temperature. The maximum scan area of MFM phase image was also  $10 \times 10 \mu\text{m}^2$ . The lift height of MFM tip was varied from 50 to 150 nm and resonant frequency of the tip was maintained approximately at 60–80 kHz. The magnetization versus magnetic field, i.e. ( $M-H$ ) measurement was recorded using vibrating sample magnetometer (Quantum Design, Versa lab 3) at room temperature. The optical properties such as absorption and transmittance spectra of BFO thin films have been recorded as the function of wavelengths using a Cary 5000 UV–Vis spectro-photometer with spectral resolution of 0.05 nm. Thickness of the annealed films prepared from molar concentration of 0.1 M, 0.3 M and 0.5 M was determined by an Ambios surface profilometer.

### 3 Results and discussion

#### 3.1 X-ray diffraction analysis

##### 3.1.1 Structural phase analysis

The representative powder X-ray diffraction (XRD) patterns of the annealed BFO thin films prepared from different molar concentrations are shown in Fig. 1. The observed all diffraction peaks of BFO thin films match well with the

JCPDS (no. 077-8894) and hence confirm the formation of orthorhombic crystal structure with Pbnm space group [79]. A single peak of impurities ( $\text{Bi}_2\text{O}_3$ ) at  $2\theta \sim 27.32^\circ$  is also observed in the XRD pattern. The occurrence of impurity phases in BFO films may be due to the instability (slow Brownian motion of the molecules) of the sol–gel at lower molar concentration of 0.1 M. However, the reflection peak of impurities ( $\text{Bi}_2\text{O}_3$ ) disappears in the XRD pattern as the molar concentration increases from 0.1 to 0.5 M. Thus, increase the molar concentration of precursor solution is helpful in suppressing the impurity phases. The characteristic diffraction peaks due to the planes such as (002), (111), (020), (200), (022), (004), (114) and (312) of  $\text{BiFeO}_3$  have been observed. The unit cell parameters are modified as the inter-planer spacing increases due to the gradual shift of diffraction peaks towards lower angle side with increase of the molar concentration. The calculated lattice parameters ( $a$ ,  $b$  and  $c$ ) and unit cell volume of BFO thin films prepared from different molar concentration of 0.1 M, 0.3 M and 0.5 M are presented in Table 1. A slight expansion of the unit cell observed in the present investigation with increase the molar concentration indicates that crystal structure is slightly modified. Further, the magnified view of the XRD pattern near  $2\theta = 32.0^\circ$  depicted in Fig. 1b shows that two very close diffraction peaks (020) and (200) are separated

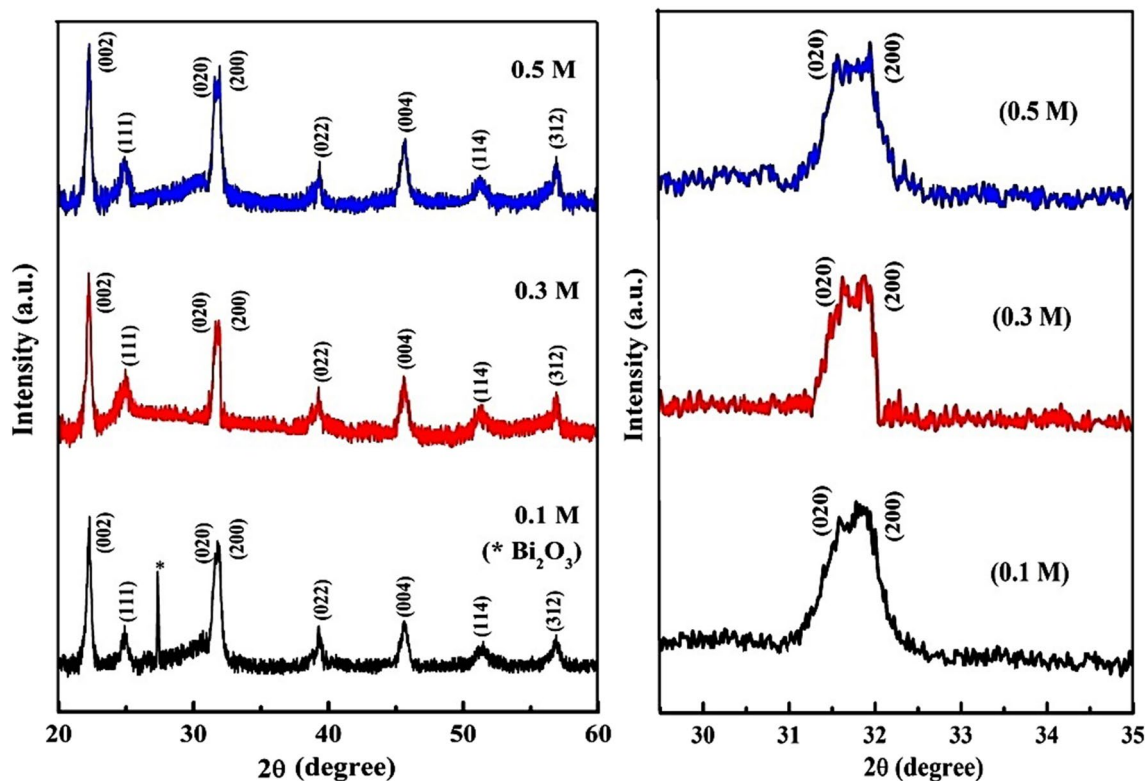


**Fig. 1** a X-ray diffraction patterns of BFO thin films deposited on glass substrate for precursor solution of molar concentration of 0.1 M, 0.3 M and 0.5 M (\*the impurity peak of  $\text{Bi}_2\text{O}_3$ ). b Magnified description of the peak around  $2\theta = 32^\circ$

**Table 1** The lattice parameters, strain, cell volume, crystallite size and texture coefficients the BFO thin film deposited from the precursor solution of various molar concentrations

BiFeO <sub>3</sub> thin films deposited from various molar concentration (M)	Lattice parameter			Lattice strain	Cell volume (Å <sup>3</sup> )	Crystallite size (nm)	Texture coefficient (TC <sub>hkl</sub> )
	a (Å)	b (Å)	c (Å)				
0.1	5.601	5.622	7.951	0.0019	250.368	15	0.924
0.3	5.606	5.628	7.959	0.0028	251.110	23	0.963
0.5	5.610	5.632	7.968	0.0062	251.753	28	1.092

appreciably as the molar concentration of precursor solutions increases from 0.1 to 0.5 M. It forces us to conclude that a distorted orthorhombic structure transforms to more symmetric orthorhombic structure.

The average crystallite size ( $D$ ) of the films was calculated using the Scherer formula:

$$D = \frac{K\lambda}{\beta \cos \theta}, \quad (1)$$

where  $K$  is constant and its value is 0.9 for the spherical shape,  $\lambda$  is the wavelength of X-ray,  $\beta$  is the full width at half maxima (FWHM) and  $\theta$  is the Bragg diffraction angle. The calculated crystallite size of the BFO films prepared from different molar concentrations of 0.1 M, 0.3 M, 0.5 M are found to be 15, 23, 28 nm, respectively. This slight expansion of unit cell and the increase of crystallite size from 15 to 28 nm with the change of molar concentrations may be due to the decrease of oxidation state of iron, i.e. from Fe<sup>3+</sup> (0.064 nm) to Fe<sup>2+</sup> (0.076 nm). It is a well-known fact that the complex 3d-metal oxides easily allow the change of oxygen stoichiometry (oxygen excess and/or deficit) [80, 81], in the present investigation, the films were prepared and annealed in air (oxygen deficit atmosphere), so oxygen deficit can decrease the oxidation state of iron (Fe).

**3.1.1.1 Williamson–Hall analysis** The more accurate crystallite size and lattice strain of each thin films were also calculated using Williamson–Hall (W–H) plots between  $\beta \cos \theta$  and  $4\sin \theta$ , as mathematically represented by

$$\beta \cos \theta = \frac{k\lambda}{D} + 4\epsilon \sin \theta. \quad (2)$$

Further, the Bragg diffraction peak width is a combination of instrumental integral width and the width broadening due to the materials. Therefore, the correct broadening of the diffraction peak of BFO thin films is estimated using the relation:

$$\beta = [\beta_{\text{measure}}^2 - \beta_{\text{instrumental}}^2]^{1/2}. \quad (3)$$

The instrumental integral width ( $\beta_{\text{instrumental}}$ ) was determined from the collected diffraction data of standard materials such as silicon. The W–H plots for BFO thin films

deposited by spin-coating method from different molar concentration are shown in Fig. 2a–c. The values of lattice strain and crystallite size of BFO thin films prepared are presented in Table 1 and the variation of crystallite size and lattice strain as a function of molar concentration are shown in Fig. 2d. It is inferred that the lattice strain increases gradually and crystallite size increases sharply with increasing molar concentration of precursor solution. This sharp variation of crystallite size creates massive dislocations within the crystal, and strain induces structural transformation from distorted orthorhombic crystal structure to single orthorhombic phase with Pbnm space group [79].

### 3.1.2 Texture coefficient analysis

The texture coefficient (TC<sub>hkl</sub>) of the ( $hkl$ ) plane of as annealed films was calculated for the evaluation of the relative degree of preferred orientation of crystallite planes, using the following equation from the X-ray diffraction data:

$$TC_{hkl} = \frac{N \left( \frac{I_{(hkl)}}{I_{0(hkl)}} \right)}{\sum \frac{I_{(hkl)}}{I_{0(hkl)}}}, \quad (4)$$

where  $I_{(hkl)}$  is the measured peak intensity and  $I_{0(hkl)}$  is the standard integral peak intensity of ( $hkl$ ) plane and  $N$  is the number of diffraction peaks observed from XRD pattern. If the texture coefficient is greater than 1, the crystal orientation is preferably oriented in particular direction. The TC<sub>hkl</sub> value was calculated for all diffraction peaks present in the XRD pattern. Depending on the molar concentration, the TC<sub>hkl</sub> values of BFO thin films for (002) peak are presented in Table 1. It can be seen that TC<sub>hkl</sub> value for (002) peak of film prepared from molar concentration of 0.1 M is 0.924 which is higher than the value for other peaks. While increasing the molar concentration from 0.1 to 0.5 M, the TC<sub>hkl</sub> value of (002) peak increases from 0.924 to 1.092. This small difference may be too small to be significant considering the quality of the XRD patterns.

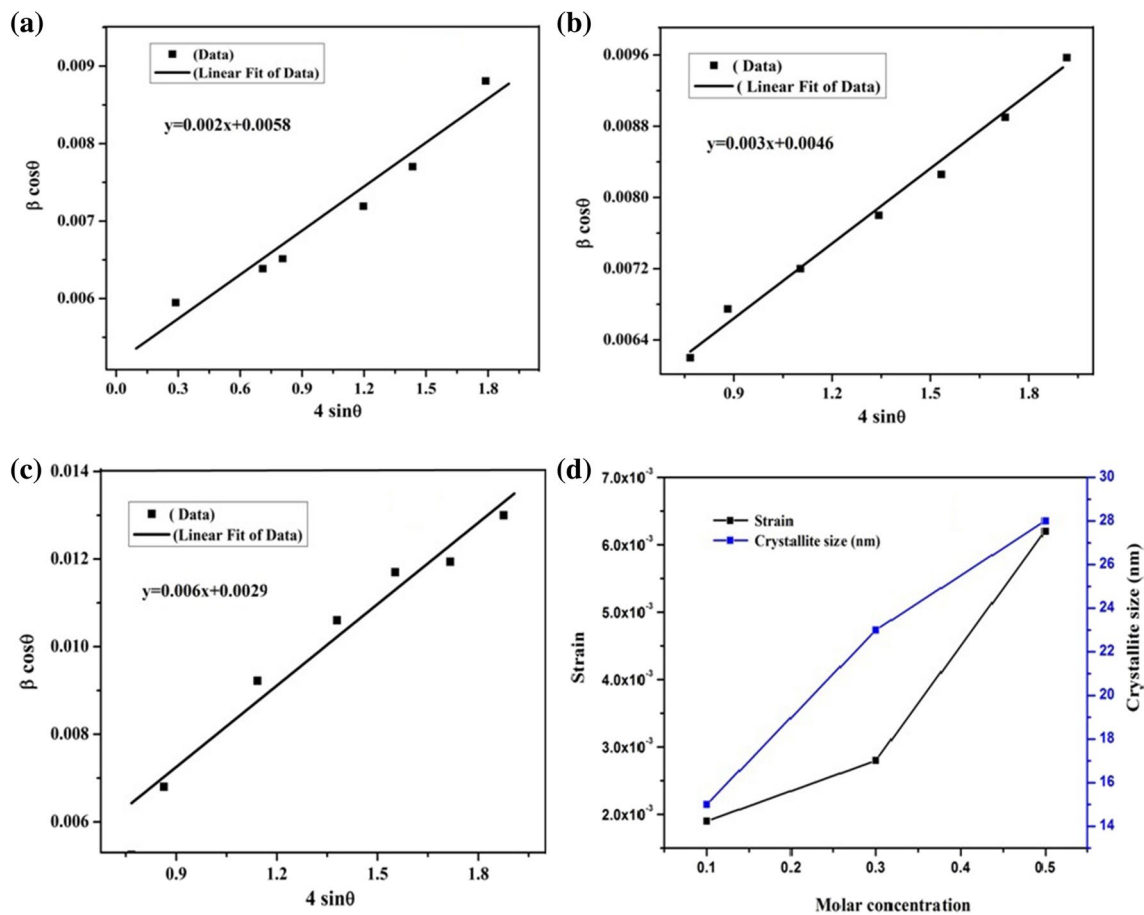


**Fig. 2** a–c Williamson–Hall plots of BFO thin films, **d** crystallite size and strain verses function of molar concentration of 0.1 M, 0.3 M and 0.5 M

### 3.2 Surface morphology and topography analyses

The field emission scanning electron micrograph (FE-SEM) and corresponding energy-dispersive X-ray spectra (EDS/EDX) of annealed thin films prepared from precursor solution of molar concentration (0.1 M and 0.5 M) are shown in Fig. 3a, b. The SEM images indicate that surface of the thin films prepared from molar concentration of 0.1 M are highly porous. This may be due to the destruction of grains by mass transport, and especially oxygen vacancy transport [82]. It may also be seen that surface contains irregular-shaped nanoparticles, well connected to each other. However, as the molar concentration increases from 0.1 to 0.5 M, the surface morphology of the films changes from granular to nanorod-like structure. The chemical composition of BFO thin films prepared from different molar concentration of 0.1 M and 0.5 M has been estimated by energy-dispersive X-ray spectroscopy (EDS or EDX). The EDS/EDX spectra shown in Fig. 3 confirms the presence of Bi, Fe and O elements in proper stoichiometry.

The surface topography of BFO thin films explored through atomic force microscopy (AFM) is shown in Fig. 4a–c. The topographic images of BFO film prepared from molar concentration of 0.1 M reveal that surface is highly porous. However, increasing the molar concentration from 0.1 to 0.3 M, the porosity is decreasing and hence improving the density of films. Furthermore, increasing the molar concentration from 0.3 to 0.5 M, the shapes of grain changes from ellipsoid to nanorods frequently observed in AFM image (4-d) of scanning area of  $4 \times 4 \mu\text{m}^2$ . The dimension of nanorods is estimated with the help of cross-sectional topographic image recorded using WSxM software and found to be  $58 \times 14 \text{ nm}^2$ . The surface roughness of the films also changes with varying molar concentration of precursor solution. The root mean square (RMS) roughness of the films has been observed using WSxM 4.0-Beta 8.2 software. The RMS roughness has been found to be 13.59, 6.34, 29.88 nm for the films prepared from molar concentrations of 0.1 M, 0.3 M, 0.5 M, respectively. The irregular variation of RMS roughness may be due to the destruction or creation of the

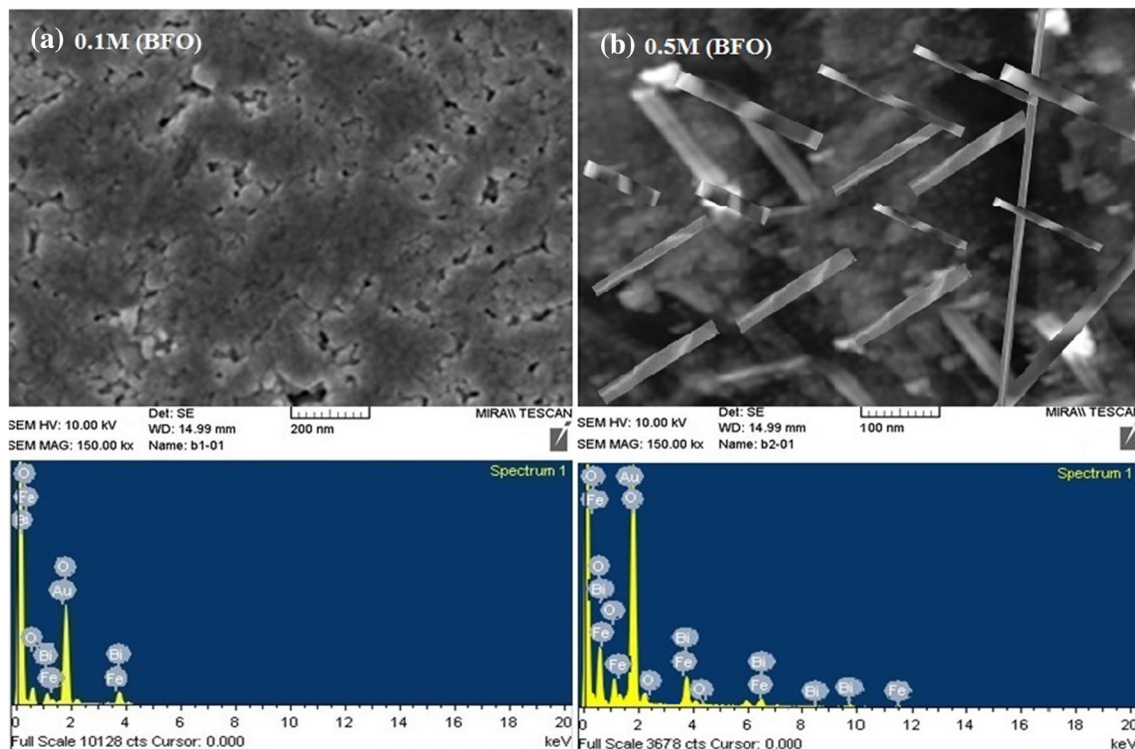


**Fig. 3** Scanning electron micrographs and EDS spectra of BFO thin films prepared from molar concentrations of **a** 0.1 M, **b** 0.5 M

grains by mass transport, and especially oxygen vacancy transport [82].

### 3.3 Magnetic domain and $M$ – $H$ measurement analysis

The microscopic local magnetic domain structure of BFO thin films have been studied using high-resolution magnetic force microscopy (MFM). Figure 5a–f shows the MFM phase image and their corresponding cross-sectional phase analysis of annealed BFO thin films prepared from different molar concentrations of 0.1 M, 0.3 M and 0.5 M. The bright–dark dipole contrast appearing in the MFM phase image clearly shows the presence of the strip-like magnetic domain with a regular and periodic arrangement. This periodic uniformity and width of the magnetic domain shown in Fig. 5a–c also increase with increase in the precursor concentration. The width enhancement of periodic domain, which is changing with the local symmetry at the domain wall, may significantly affect the magnetic properties. Such magnetic behaviour is generally observed [83] when the size of the particles is lesser than the size of spiral ordering (about 62 nm). This improved ferromagnetism may be attributed by destroying the cycloid spin ordering. Also, the bright–dark dipole contrast changed into the partially dark contrast with the variation of molar concentration

from 0.1 to 0.5 M. It may be due to rotation of magnetization axis and it is consistent with the earlier report [84] in which the change in width and directions of the domain had been observed. The cross-sectional phase contrast of the films deposited from the different molar concentrations of 0.1 M, 0.3 M and 0.5 M shown in Fig. 5d–f, changes from  $+0.4^\circ$  to  $-0.4^\circ$ ,  $+0.55^\circ$  to  $-0.55^\circ$  and  $+0.8^\circ$  to  $-0.9^\circ$ , respectively. Interestingly, the increased phase contrast from  $+0.8^\circ$  to  $-0.9^\circ$  shown in Fig. 5f may be attributed due to the attractive forces acting on the magnetic tip by the nanorods ( $58 \times 14 \text{ nm}^2$ ).

Further, the microscopic analysis of magnetic properties of thin films, the measurement of magnetization ( $M$ ) as a function of magnetic field ( $H$ ) was further carried out at room temperature. The exaggerated hysteresis loops of the films deposited from different molar concentration, i.e. 0.1 M, 0.3 M and 0.5 M, clearly demonstrate that the BFO thin films have a weak ferromagnetic behaviour. As already discussed in Sect. 3.1, oxygen deficit can decrease the oxidation state of iron from  $\text{Fe}^{3+}$  to  $\text{Fe}^{2+}$  [80, 81]. The change of valence state of Fe as a consequence of oxygen deficit changes the magnetic parameters such as total magnetic moment and Curie point. Moreover, oxygen vacancies also effect the exchange interactions. Intensity of exchange interactions decreases with oxygen vacancy concentration increase. In complex oxides, there is only

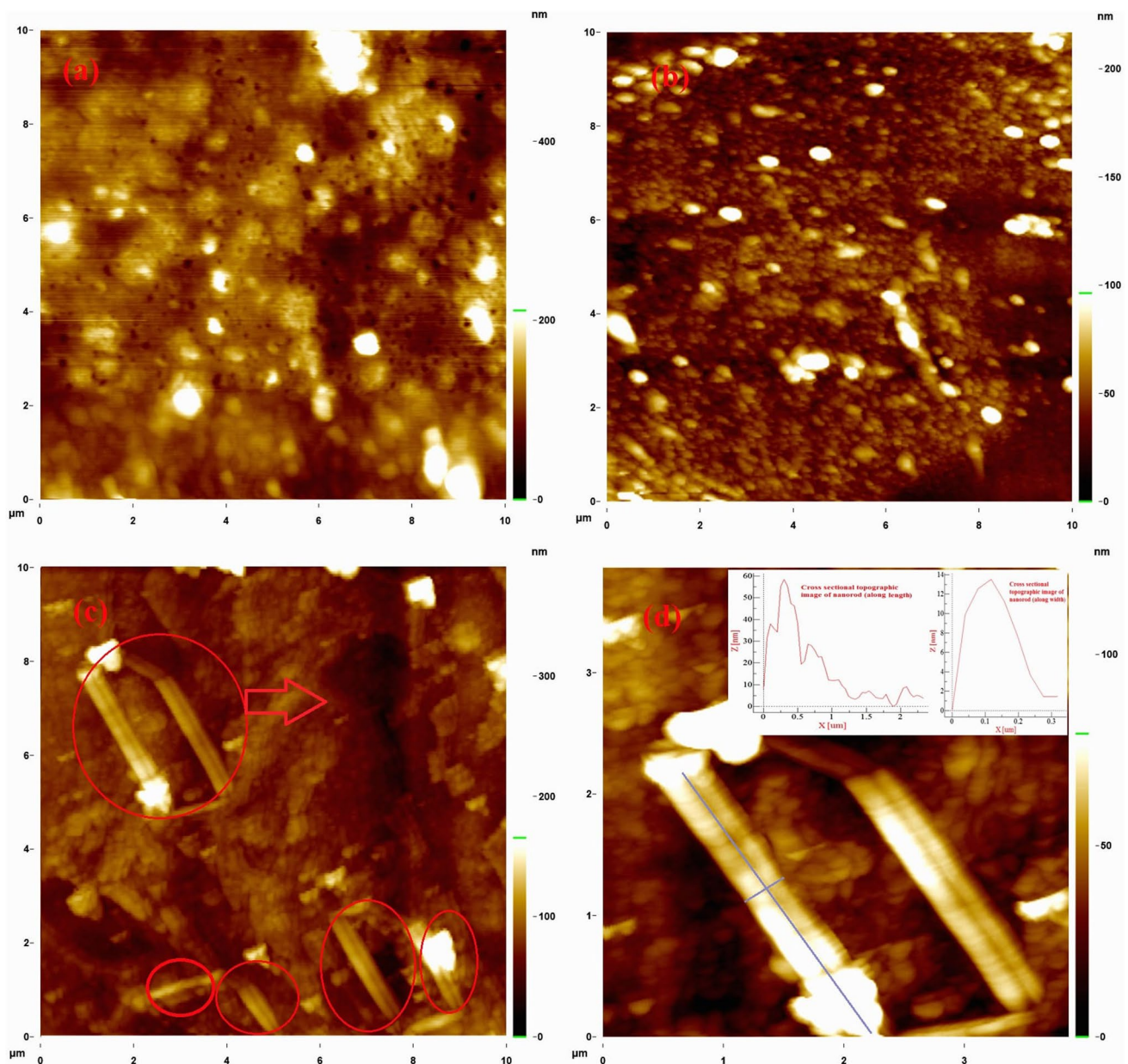


**Fig. 4** a–c AFM topographic images of BFO thin films prepared from molar concentrations of 0.1 M, 0.3 M and 0.5 M. **d** Magnified image of nanorods

indirect exchange. Exchange near the oxygen vacancies is negative according to Goodenough–Kanamori empirical rules. So oxygen vacancies should lead to the formation of a weak magnetic state such as spin glass, which we observe from Fig. 6 by the magnitude of the residual moment of  $< 0.2 \text{ emu/cm}^3$ . Thus, one can conclude that oxygen-deficit and the mixed-valence state of Fe (+2 and +3) are likely responsible for weak ferromagnetism in BFO samples. Further, the spin glass state may arise as a consequence of either a very small crystallite sizes of 15–28 nm or an inhomogeneous distribution of cationic

composition [85, 86]. However, in our case, it is due to the increase of small crystallite size from 15 to 28 nm with increase of molar concentration. This enhancement of crystallite size increases the thickness of the films from 398 to 430 nm as we observed in the present investigation. Thus, the enhancement of thickness (increase of crystallite size) of the films is responsible for the spin glass behaviour as it is reported [87]. Further, the observed remnant magnetization ( $M_r$ ) and coercivity ( $H_c$ ) of the films deposited from the different molar concentration of 0.1 M, 0.3 M, 0.5 M were found to be 0.10, 0.16, 0.19  $\text{emu/cm}^3$

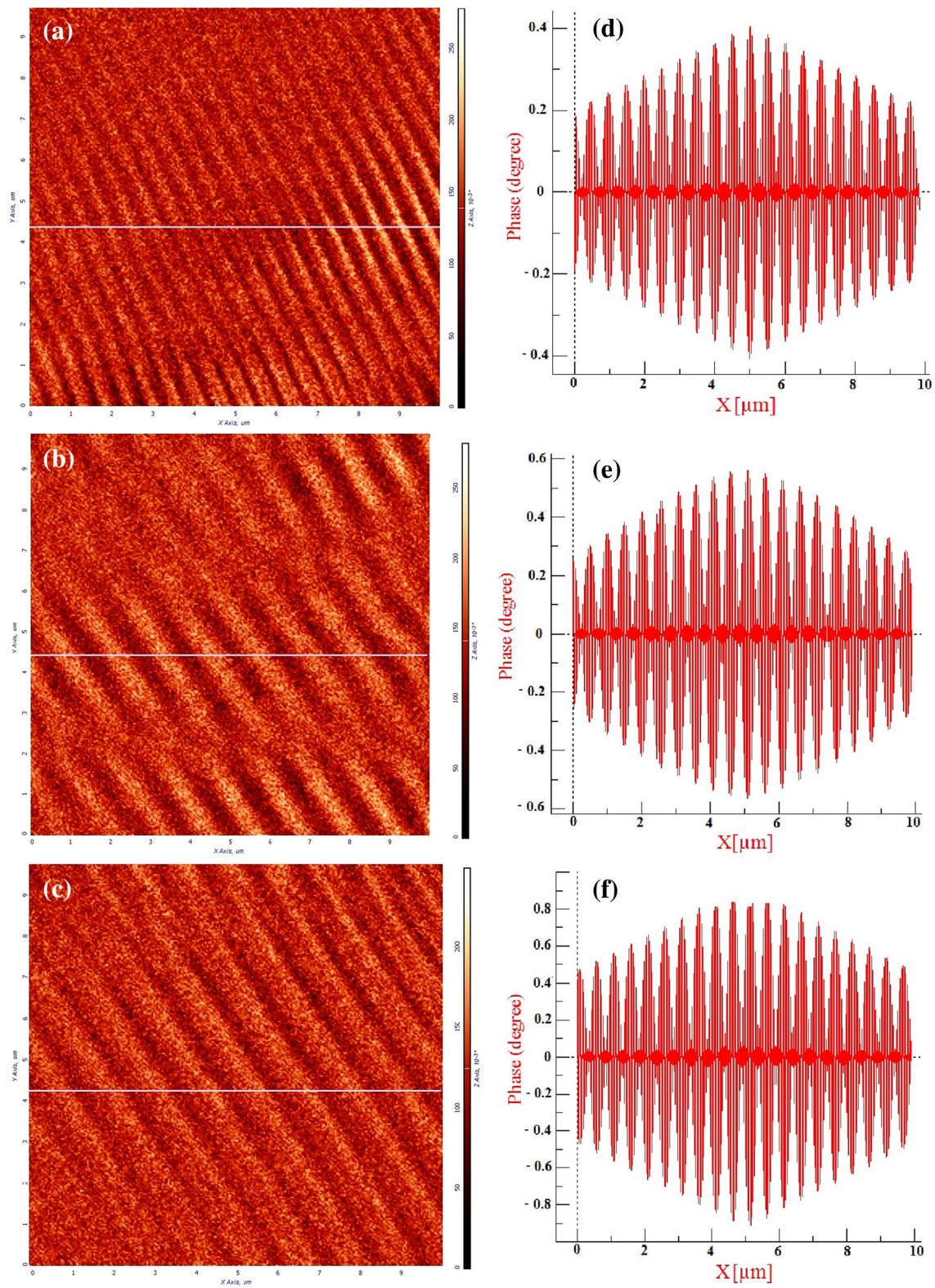


**Fig. 5** a–c MFM phase image. d–f The corresponding MFM cross-sectional phase image of BFO thin films, prepared from molar concentration of 0.1 M, 0.3 M, and 0.5 M



**Fig. 6** **a**  $M-H$  hysteresis loop, **b** the magnified view of  $M-H$  hysteresis loop of BFO thin films prepared from molar concentration of 0.1 M, 0.3 M and 0.5 M

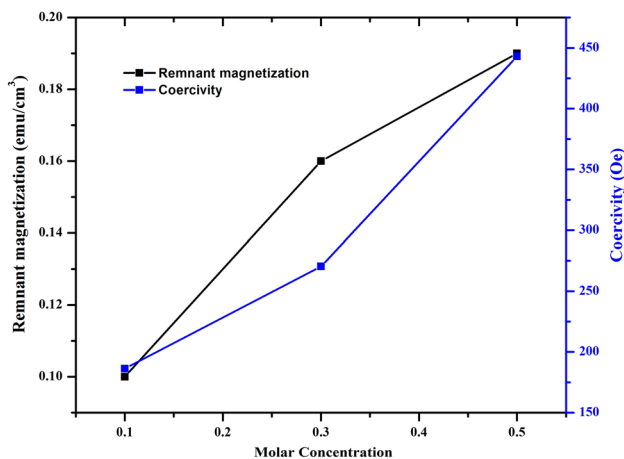
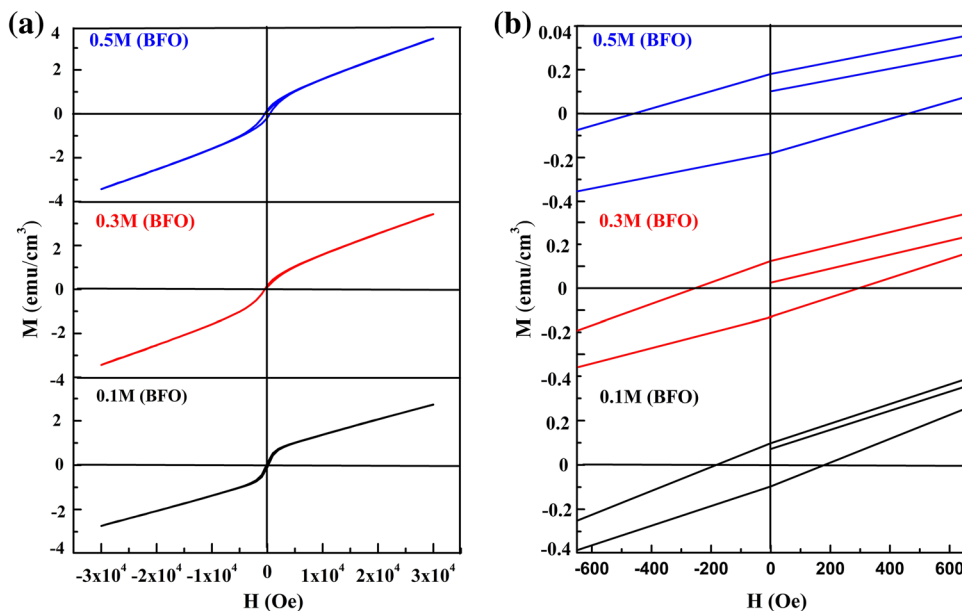


**Fig. 7** The variation of magnetic remnant magnetization ( $M_r$ ) and coercivity ( $H_c$ ) versus function of molar concentrations 0.1 M, 0.3 M and 0.5 M

and 186.24, 270.43, 443.06 Oe, respectively. The gradual increment of both the remnant magnetization ( $M_r$ ) from 0.10 to 0.19 emu/cm<sup>3</sup> and saturation magnetization ( $M_s$ ) from 2.8 to 3.6 emu/cm<sup>3</sup> with increase of the molar concentration from 0.1 to 0.5 M may be attributed due to the

formation of nanorods on the surface [88]. The enhancement of  $M_r$  and  $M_s$  of BFO thin films can be explained due to suppression of the cycloid spin structure. The variation of remnant magnetization ( $M_r$ ) and coercivity ( $H_c$ ) with different molar concentration is shown in Fig. 7. Thus, the precursor concentration plays a vital role in the formation of nanorods which consequently influence the magnetic properties.

### 3.4 Electrical properties

The electrical properties of BFO thin films deposited from different molar concentration of 0.1 M, 0.3 M and 0.5 M have been measured using Hall switching card employing van der Pauw geometry. The calculated carrier concentration and magnetoresistance value have been summarized in Table 2. Here the magnetoresistance increases from  $2.83 \times 10^8 \Omega$  to  $4.06 \times 10^9 \Omega$  with increase of the molar concentration of precursor solution from 0.1 to 0.5 M may indirectly improve the local magnetoelectric effect which plays a vital role in the domain switching behaviour of BFO materials [89].

**Table 2** The optical, electrical, surface and magnetic parameters for BiFeO<sub>3</sub> thin films prepared from precursor solution of various molar concentrations

BiFeO <sub>3</sub> thin films (M)	Optical bandgap (eV)	Carrier concentration (cm <sup>-3</sup> )	RMS roughness (nm)	Coercivity ( $H_c$ ) Oe	Remanent magnetization ( $M_r$ ) emu/cm <sup>3</sup>	Magnetoresistance ( $\Omega$ )
0.1	2.58	$1.89 \times 10^{12}$	13.59	186.24	0.10	$2.83 \times 10^8$
0.3	2.53	$7.84 \times 10^{11}$	6.34	270.43	0.16	$7.85 \times 10^8$
0.5	2.49	$2.34 \times 10^{11}$	29.88	443.06	0.19	$4.06 \times 10^9$

### 3.5 Optical properties

The absorption spectra of BFO thin films deposited on glass substrates with different molar concentration of precursor solution from 0.1 to 0.5 M are shown in Fig. 8a. The absorption spectrum of BFO thin films exhibits a sharp absorption edge at  $\sim 487$  nm. Figure 8b shows transmittance spectra for BFO films deposited on glass substrates with different molar concentration of precursor solution as a function of wavelength. The thickness values were found to be of 398, 405 and 430 nm for BFO films prepared from the molar concentration of 0.1 M, 0.3 M and 0.5 M, respectively. The BFO films prepared from 0.1 M are showing 33% transmittance due to good structural homogeneity and lower thickness. The transmittance decreases from 33 to 29% as the molar concentration of precursor increases from 0.1 to 0.3 M,

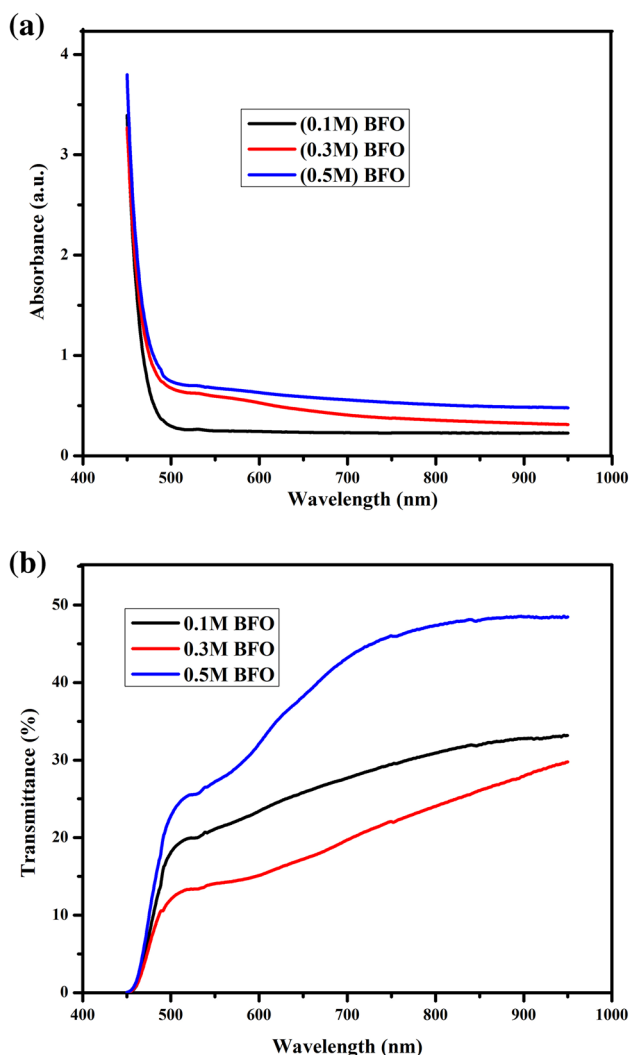


**Fig. 8** **a** The absorption spectra, **b** transmittance spectra of BFO thin films as a function of the molar concentration from 0.1 M, 0.3 M and 0.5 M

whereas transmittance increases from 29 to 48% as the molar concentration of precursor solution increases from 0.3 to 0.5 M. This may be associated with the surface roughness of the films. The BFO is natural n-type materials as confirmed from Hall measurement and the occupancy of the states near the bottom of the conduction band by the donor electrons. The optical energy gap in the oxide materials for direct transitions is defined in terms of the unperturbed energy bands:

$$E_g = E_c^o(k_F) - E_v^o(k_F), \quad (5)$$

where  $E_g$  is the bandgap,  $E_v^o(k_F)$  is unperturbed valence band and  $E_c^o(k_F)$  is unperturbed conduction bands, as well as  $k_F$  is Fermi wave vector,  $k_F = (3\pi^2 n)^{1/3}$ ,

$$E_v^o(k_F) = \left| \frac{\hbar^2 k_F^2}{2m_v^*} \right|, \quad (6)$$

$$E_c^o(k_F) = E_{go} + \left| \frac{\hbar^2 k_F^2}{2m_c^*} \right|. \quad (7)$$

Neglecting the electron–electron interactions the optical bandgap is

$$E_g = E_{go} + \frac{\hbar^2 (3\pi^2 n)^{2/3}}{2m_{vc}^*}, \quad (8)$$

where  $n$  is the carrier concentration and  $m_{vc}^*$  the effective mass of electron and holes.

The experimental value of the carrier concentration of BFO thin films deposited with different precursor concentration was already determined from the Hall measurement and presented in Table 2. The optical bandgap  $E_g$  of BFO thin films can be determined from the spectral dependence of the absorption coefficient by the application of existing theories. It is well known that the absorption coefficient ( $\alpha$ ) depends on the transition of carriers from valence to conduction band via the absorption of photons. Since the absorption spectra of BFO thin films are reported to be endorsed to the direct transition, so the absorption coefficient ( $\alpha$ ) obeys the Tauc relation:

$$\alpha h\nu = A \left( h\nu - E_g \right)^n, \quad (10)$$

where  $h\nu$  is photon energy,  $E_g$  is the optical bandgap and  $A$  is a correction coefficient which depends on different values of  $n$ . The significance of  $n$  is correlated with different types of electronic transitions and the values of  $n$  are 1/2 and 2/3 for direct bandgap-forbidden and -allowed transitions, respectively, while for indirect bandgap-forbidden and -allowed transition,  $n = 2$  and 3, respectively. The variation of  $(\alpha h\nu)^2$  with  $(h\nu)$  is shown in Fig. 9 and the optical bandgap ( $E_g$ ) was estimated by extrapolation of the linear part of the curves.

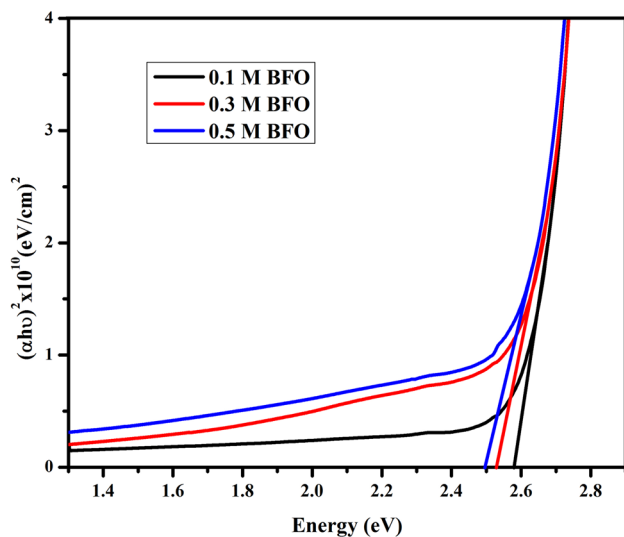


**Fig. 9** Plots of  $(\alpha h\nu)^2$  versus  $(h\nu)$  of BFO thin films

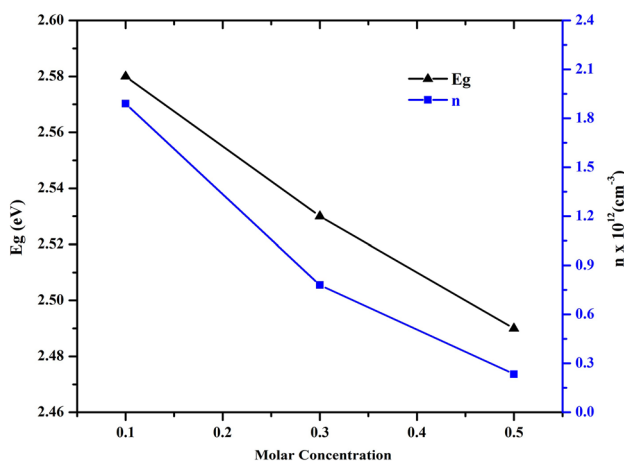


**Fig. 10** Plot of carrier concentration ( $n$ ) and optical bandgap ( $E_g$ ) versus function of molar concentration

The optical bandgaps of BFO thin films prepared from molar concentration of 0.1 M, 0.3 M and 0.5 M were found to be 2.58, 2.53 and 2.49 eV, respectively. The change of carrier concentration and optical bandgap with precursor molar concentration is shown in Fig. 10. It is clearly evidenced from curves that both carrier concentration and optical bandgap decreases with increase of the precursor molar concentration due to the electron–electron interactions. This is well consistent with Eq. (8). The variation of optical bandgap may also be correlated with the change in crystallite size.

## 4 Conclusions

In the present paper, BFO thin films are deposited on glass substrates with different molar concentrations by the spin-coating technique. The XRD analysis shows a phase transformation from distorted orthorhombic to single orthorhombic phase with increase of the molar concentration from 0.1 to 0.5 M. The SEM/AFM image reveals the formation of nanorods on the surface of BFO thin films deposited from the molar concentration of 0.5 M. The RMS roughness value of the BFO films was observed to be 13.59, 6.34 and 29.88 nm, respectively. The MFM phase images revealed the periodic and strip-like structure of magnetic domain. The bright and dark contrasts of magnetic domains indicate the electric-field-induced rotation of magnetization axis, i.e. indirect magnetoelectric coupling exists at room temperature. The optical bandgap of BFO thin films was found to decrease from 2.58 to 2.49 eV with increasing molar concentration from 0.1 to 0.5 M. This decrement in optical bandgap may be due to the increment of crystallite size from 15 to 28 nm. From  $M$ – $H$  measurements, the remnant magnetization ( $M_r$ ) and coercivity ( $H_C$ ) of BFO thin films deposited from molar concentration of 0.1 M, 0.3 M, 0.5 M were found to be 0.10, 0.16, 0.19 emu/cm<sup>3</sup> and 186.24, 270.43 and 443.06 Oe, respectively. The suppression of the cycloid spin ordering due to formation of nanorods in the films prepared from molar concentration of 0.5 M may be responsible for the improvement of magnetic properties of BiFeO<sub>3</sub> thin films.

**Acknowledgements** We are very much grateful to Prof. O. N. Srivastava, Department of Physics, Banaras Hindu University, India, for fruitful discussions. The authors are also thankful to the UGC-DAE-CSR at Indore and Inter-University Accelerator Centre (IUAC), New Delhi, India, for providing the various characterization facilities.

## References

1. R. Ramesh, Emerging routes to multiferroics. *Nature* **461**, 1218–1219 (2009)
2. G. Catalan, J.F. Scott, Physics and applications of bismuth ferrite. *Adv. Mater.* **21**, 2463–2485 (2009)
3. N.A. Spaldin, M. Fiebig, The renaissance of magnetoelectric multiferroics. *Science* **309**, 391–392 (2005)
4. W. Eerenstein, N.D. Mathur, J.F. Scott, Multiferroic and magnetoelectric materials. *Nature* **442**, 759–765 (2006)
5. S.W. Cheong, M. Mostovoy, Multiferroics a magnetic twist for ferroelectricity. *Nat. Mater.* **6**, 13–20 (2007)
6. A. Reyes, A.C. de la Vega, M.E. Fuentes, L. Fuentes, BiFeO<sub>3</sub> synchrotron radiation structure refinement and magnetoelectric geometry. *J. Eur. Ceram. Soc.* **27**, 3709 (2007)
7. S. Fujino, M. Murakami, S.-H. Lim, L.G. Salamanca-Riba, M. Wuttig, I. Takeuchia, Multiphase growth in Bi–Mn–O thin films. *J. Appl. Phys.* **101**, 013903 (2007)

8. Z.H. Sun, B.L. Cheng, S. Dai, L.Z. Cao, Y.L. Zhou, K.J. Jin, Z.H. Chen, G.Z. Yang, Dielectric property studies of multiferroic  $\text{GaFeO}_3$ . *J. Phys. D Appl. Phys.* **39**, 2481–2484 (2006)
9. O.P. Vajk, M. Kenzelmann, J.W. Lynn, S.B. Kim, S.W. Cheong, Magnetic order and spin dynamics in ferroelectric  $\text{HoMnO}_3$ . *PRL* **94**, 087601 (2005)
10. D. Senff, N. Aliouane, D.N. Argyriou, A. Hiess, L.P. Regnault, P. Link, K. Hradil, Y. Sidis, M. Braden, Magnetic excitations in a cycloidal magnet the magnon spectrum of multiferroic  $\text{TbMnO}_3$ . *J. Phys. Condens. Matter.* **20**, 434212 (2008)
11. C. Ederer, N.A. Spaldin, Weak ferromagnetism and magnetoelectric coupling in bismuth ferrite. *Phys. Rev. B* **71**, 060401 (2005)
12. J.T. Haraldsen, A.V. Balatsky, Effects of magnetoelectric ordering due to interfacial symmetry breaking. *Mater. Res. Lett.* **1**, 39–44 (2013)
13. W. Ratcliff, J.W. Lynn, V. Kiryukhin, P. Jain, M.R. Fitzsimmons, Magnetic structures and dynamics of multiferroic systems obtained with neutron scattering. *Nat. Commun.* **1**, 16003 (2016)
14. P. Ravindran, R. Vidya, A. Kjekshus, H. Fjellvåg, O. Eriksson, Theoretical investigation of magnetoelectric behavior in  $\text{BiFeO}_3$ . *Phys. Rev. B* **74**, 224412 (2006)
15. A.V. Trukhanov, V.O. Turchenko, I.A. Bobrikov, S.V. Trukhanov, I.S. Kazakevich, A.M. Balagurov, Crystal structure and magnetic properties of the  $\text{BaFe}_{12-x}\text{Al}_x\text{O}_{19}$  ( $x = 0.1-1.2$ ) solid solutions. *J. Magn. Magn. Mater.* **393**, 253–259 (2015)
16. S.V. Trukhanov, A.V. Trukhanov, V.A. Turchenko, V.G. Kostishyn, L.V. Panina, I.S. Kazakevich, A.M. Balagurov, Crystal structure and magnetic properties of the  $\text{BaFe}_{12-x}\text{In}_x\text{O}_{19}$  ( $x = 0.1-1.2$ ) solid solutions. *J. Magn. Magn. Mater.* **417**, 130–136 (2016)
17. S.V. Trukhanova, A.V. Trukhanova, V.G. Kostishyn, L.V. Panina, V.A. Turchenko, I.S. Kazakevich, An.V. Trukhanova, E.L. Trukhanov, V.O. Natarov, A.M. Balagurov, Thermal evolution of exchange interactions in lightly doped barium hexaferrites. *J. Magn. Magn. Mater.* **426**, 554–562 (2017)
18. S.V. Trukhanov, A.V. Trukhanov, V.A. Turchenko, V.G. Kostishyn, L.V. Panina, I.S. Kazakevich, A.M. Balagurov, Structure and magnetic properties of  $\text{BaFe}_{11.9}\text{In}_{0.1}\text{O}_{19}$  hexaferrite in a wide temperature range. *J. Alloys Compd.* **689**, 383–393 (2016)
19. A.V. Trukhanov, S.V. Trukhanov, L.V. Panina, V.G. Kostishyn, I.S. Kazakevich, An.V. Trukhanov, E.L. Trukhanova, V.O. Natarov, V.A. Turchenko, M.M. Salem, A.M. Balagurov, Evolution of structure and magnetic properties for  $\text{BaFe}_{11.9}\text{Al}_{0.1}\text{O}_{19}$  hexaferrite in a wide temperature range. *J. Magn. Magn. Mater.* **426**, 487–496 (2017)
20. S.V. Trukhanov, A.V. Trukhanov, L.V. Panina, V.G. Kostishyn, V.A. Turchenko, E.L. Trukhanova, An.V. Trukhanov, T.I. Zubar, V.M. Ivanov, D.I. Tishkevich, D.A. Vinnik, S.A. Gudkova, D.S. Klygach, M.G. Vakhitov, P. Thakur, A. Thakur, Y. Yang, Temperature evolution of the structure parameters and exchange interactions in  $\text{BaFe}_{12-x}\text{In}_x\text{O}_{19}$ . *J. Magn. Magn. Mater.* **466**, 393–405 (2018)
21. X. Xu, W. Liu, H. Zhang, M. Guo, P. Wu, S. Wang, J. Gao, G. Rao, The abnormal electrical and optical properties in Na and Ni codoped  $\text{BiFeO}_3$  nanoparticles. *J. Appl. Phys.* **117**, 174106 (2015)
22. J. Wang, J.B. Neaton, H. Zheng, V. Nagarajan, S.B. Ogale, B. Liu, D. Viehland, V. Vaithyanathan, D.G. Schlom, U.V. Waghmare, N.A. Spaldin, K.M. Rabe, M. Wuttig, R. Ramesh, Epitaxial  $\text{BiFeO}_3$  multiferroic thin film heterostructures. *Science* **299**, 1719–1722 (2003)
23. L.W. Martin, Y.H. Chu, M.B. Holcomb, M. Huijben, P. Yu, S.J. Han, D. Lee, S.X. Wang, R. Ramesh, Nanoscale control of exchange bias with  $\text{BiFeO}_3$  thin films. *Nano Lett.* **8**, 2050–2055 (2008)
24. V.A. Reddy, N.P. Pathak, R. Nath, Particle size dependent magnetic properties and phase transition in multiferroic  $\text{BiFeO}_3$  nanoparticles. *J. Alloy. Compd.* **543**, 206–212 (2012)
25. T.J. Park, G.C. Papaefthymiou, A.J. Viescas, A.R. Moodenbaugh, S.S. Wong, Size-dependent magnetic properties of single-crystalline multiferroic  $\text{BiFeO}_3$  nanoparticles. *Nano Lett.* **7**, 766–772 (2007)
26. J.B. Neaton, C. Ederer, U.V. Waghmare, N.A. Spaldin, K.M. Rabe, First-principles study of spontaneous polarization in multiferroic  $\text{BiFeO}_3$ . *Phys. Rev. B* **71**, 014113 (2005)
27. A.N. Morozovska, R.K. Vasudevan, P. Maksymovych, S.V. Kalinin, E.A. Eliseev, Anisotropic conductivity of uncharged domain walls in  $\text{BiFeO}_3$ . *Phys. Rev. B. Condens. Matter* **86**, 085315 (2012)
28. A.V. Trukhanov, S.V. Trukhanov, L.V. Panina, V.G. Kostishyn, D.N. Chitanov, I.S. Kazakevich, A.V. Trukhanov, V.A. Turchenko, Strong correlation between magnetic and electrical subsystems in diamagnetically substituted hexaferrites ceramics. *Ceram. Int.* **43**, 5635–5641 (2017)
29. A.V. Trukhanov, S.V. Trukhanov, V.G. Kostishyn, L.V. Panina, M.M. Salem, I.S. Kazakevich, V.A. Turchenko, V.V. Kochervinskii, D.A. Krivchenya, Multiferroic properties and structural features of M-type Al-substituted barium hexaferrites. *Phys. Solid State* **59**, 737–745 (2017)
30. S.V. Trukhanov, A.V. Trukhanov, V.A. Turchenko, An.V. Trukhanov, E.L. Trukhanova, D.I. Tishkevich, V.M. Ivanov, T.I. Zubar, M. Salem, V.G. Kostishyn, L.V. Panina, D.A. Vinnik, S.A. Gudkova, Polarization origin and iron positions in indium doped barium hexaferrites. *Ceram. Int.* **44**, 290–300 (2018)
31. S.V. Trukhanov, A.V. Trukhanov, V.A. Turchenko, An.V. Trukhanov, D.I. Tishkevich, E.L. Trukhanova, T.I. Zubar, D.V. Karpinsky, V.G. Kostishyn, L.V. Panina, D.A. Vinnik, S.A. Gudkova, E.A. Trofimov, P. Thakur, A. Thakur, Y. Yang, Magnetic and dipole moments in indium doped barium hexaferrites. *J. Magn. Magn. Mater.* **457**, 83–96 (2018)
32. X.W. Tang, J.M. Dai, X.B. Zhu, J.C. Lin, Q. Chang, D.J. Wu, W.H. Song, Y.P. Sun, Thickness-dependent dielectric, ferroelectric, and magneto dielectric properties of  $\text{BiFeO}_3$  thin films derived by chemical solution deposition. *J. Am. Ceram. Soc.* **95**, 538–544 (2012)
33. J.P. de la Cruz, E. Joanni, P.M. Vilarinho, A.L. Kholkin, Thickness effect on the dielectric, ferroelectric, and piezoelectric properties of ferroelectric lead zirconate titanate thin films. *J. Appl. Phys.* **108**, 114106 (2010)
34. T.M. Shaw, S. Trolier-McKinstry, P.C. McIntyre, The properties of ferroelectric films at small dimensions. *Annu. Rev. Mater. Sci.* **30**, 263–298 (2000)
35. R. Kretschmer, K. Binder, Surface effects on phase-transitions in ferroelectrics and dipolar magnets. *Phys. Rev. B* **20**, 1065–1076 (1979)
36. J.P. Zhou, R.J. Xiao, Y.X. Zhang, Z.H. Shi, G.Q. Zhu, Novel behaviors of single crystalline  $\text{BiFeO}_3$  nanorods hydrothermally synthesized under magnetic field. *J. Mater. Chem. C.* **3**, 6924–6931 (2015)
37. W.J. Luo, D.L. Wang, F.W. Wang, T. Liu, J.W. Cai, L.Y. Zhang, Y.L. Liu, Room temperature simultaneously enhanced magnetization and electric polarization in  $\text{BiFeO}_3$  ceramic synthesized by magnetic annealing. *Appl. Phys. Lett.* **94**, 202507 (2009)
38. X.W. Tang, J.M. Dai, X.B. Zhu, H.C. Lei, L.H. Yin, W.H. Song, Y.L. Cheng, D.J. Wu, Y.P. Sun, Magnetic field annealing effects on self-oriented  $\text{BiFeO}_3$  thin films prepared by chemical solution deposition. *J. Magn. Magn. Mater.* **322**, 2647–2652 (2010)
39. S.K. Jim, J.W. Jeong, J.W. Lee, S.C. Shin, Enhancement of saturation magnetization in epitaxial (111)  $\text{BiFeO}_3$  films by magnetic annealing. *Thin Solid Films* **517**, 2749–2752 (2009)
40. Y. Wang, R. Zheng, C. Sim, J. Wang, Charged defects and their effects on electrical behaviour in  $\text{Bi}_{1-x}\text{La}_x\text{FeO}_3$  thin films. *J. Appl. Phys.* **105**, 016106 (2009)

41. W.H. Kim, J.Y. Son, The effects of La substitution on ferroelectric domain structure and multiferroic properties of epitaxially grown BiFeO<sub>3</sub> thin films. *Appl. Phys. Lett.* **103**, 132907 (2013)
42. N.V. Minh, D.V. Thang, Dopant effects on the structural, optical and electromagnetic properties in multiferroic Bi<sub>1-x</sub>Y<sub>x</sub>FeO<sub>3</sub> ceramics. *J. Alloy. Comp.* **505**, 619–622 (2010)
43. A. Gautam, V.S. Rangra, Effect of Ba ions substitution on multiferroic properties of BiFeO<sub>3</sub> perovskite. *Cryst. Res. Technol.* **45**, 953–956 (2010)
44. P.C. Sati, M. Kumar, S. Chhoker, Low temperature ferromagnetic ordering and dielectric properties of Bi<sub>1-x</sub>Dy<sub>x</sub>FeO<sub>3</sub> ceramics. *Ceram. Int.* **41**, 3227–3236 (2015)
45. B. Bhushan, Z. Wang, J. van Tol, N.S. Dalal, A. Basumallick, N.Y. Vasanthacharya, S. Kumar, D. Das, Tailoring the magnetic and optical properties of nanocrystalline BiFeO<sub>3</sub> by Ce doping. *J. Am. Ceram. Soc.* **95**, 1985–1992 (2012)
46. R. Das, K. Mandal, Magnetic, ferroelectric and magnetoelectric properties of Ba-doped BiFeO<sub>3</sub>. *J. Magn. Mater.* **324**, 1913–1918 (2012)
47. W. Liu, G. Tan, G. Dong, X. Yan, W. Ye, H. Ren, A. Xia, Structure transition and multiferroic properties of Mn-doped BiFeO<sub>3</sub> thin films. *J. Mater. Sci. Mater. Electron.* **25**, 723–729 (2014)
48. J. Wu, J. Wang, D. Xiao, J. Zhu, Migration kinetics of oxygen vacancies in Mn-modified BiFeO<sub>3</sub> thin films. *ACS Appl. Mater. Interfaces* **3**, 2504–2511 (2011)
49. H. Naganuma, J. Miura, S. Okamura, Annealing temperature effect on ferroelectric and magnetic properties in Mn-added polycrystalline BiFeO<sub>3</sub> films. *J. Electroceram.* **22**, 203–208 (2009)
50. D. Kothari, V.R. Reddy, A. Gupta, D.M. Phase, N. Lakshmi, S.K. Deshpande, A.M. Awasthi, Study of the effect of Mn doping on the BiFeO<sub>3</sub> system. *J. Phys. Condens. Matter.* **19**, 136202 (2007)
51. S. Chauhan, M. Kumar, S. Chhoker, S.C. Katyala, H. Singh, M. Jewariya, K.L. Yadav, Multiferroic, magnetoelectric and optical properties of Mn doped BiFeO<sub>3</sub> nanoparticles. *Solid State Commun.* **152**, 525 (2012)
52. T. Kawae, H. Tsuda, H. Naganuma, S. Yamada, M. Kumeda, S. Okamura, A. Morimoto, Composition dependence in BiFeO<sub>3</sub> film capacitor with suppressed leakage current by Nd and Mn cosubstitution and their ferroelectric properties. *Jpn. J. Appl. Phys.* **47**, 7586–7589 (2008)
53. F. Yan, G. Zhao, N. Song, N. Zhao, Y. Chen, In situ synthesis and characterization of fine-patterned La and Mn co-doped BiFeO<sub>3</sub> film. *J. Alloys Compd.* **570**, 19–22 (2013)
54. J. Kolte, A. Daryapurkar, P. Apte, P. Gopalan, Structural and electrical characterization of La and Mn co-substituted bismuth ferrite thin films. *Ferroelectrics* **448**, 42–49 (2013)
55. H. Liu, P. Yang, K. Yao, J. Wang, Twinning rotation and ferroelectric behaviour of epitaxial BiFeO<sub>3</sub> (001) thin film. *Appl. Phys. Lett.* **96**, 012901 (2010)
56. A.R. Venkateswarlu, G.D. Varma, R. Nath, Optical and electrical properties of spray pyrolysis deposited nano-crystalline BiFeO<sub>3</sub> films. *AIP Adv.* **1**, 042140 (2011)
57. D. Huang, H. Deng, P. Yang, J. Chu, Optical and electrical properties of multiferroic bismuth ferrite thin films fabricated by sol-gel technique. *Mater. Lett.* **64**, 2233–2235 (2010)
58. J. Liua, H. Dengb, L. Zhua, K. Zhanga, X. Menga, H. Caoa, P. Yanga, J. Chu, Structure, optical and magnetic properties of Bi<sub>1-x</sub>Eu<sub>x</sub>FeO<sub>3</sub> films fabricated by pulsed laser deposition. *Appl. Surf. Sci.* **316**, 78–81 (2014)
59. F. Huang, X. Lu, W. Lin, X. Wu, Y. Kan, J. Zhu, Effect of Nd dopant on magnetic and electric properties of BiFeO<sub>3</sub> thin films prepared by metal organic deposition method. *Appl. Phys. Lett.* **89**, 242914 (2006)
60. H. Yang, Y.Q. Wang, H. Wang, Q.X. Jia, Oxygen concentration and its effect on the leakage current in BiFeO<sub>3</sub> thin films. *Appl. Phys. Lett.* **96**, 012909 (2010)
61. S.K. Singh, H. Ishiwara, Reduced leakage current in BiFeO<sub>3</sub> thin films on Si substrates formed by a chemical solution method. *Jpn. J. Appl. Phys.* **44**, 734–736 (2005)
62. S.Y. Yang, F. Zavaliche, L. Mohaddes-Ardabili, V. Vaithyanathan, D.G. Schlom, Y.J. Lee, Y.H. Chu, M.P. Cruz, Q. Zhan, T. Zhao, R. Ramesh, Metallorganic chemical vapor deposition of lead-free ferroelectric BiFeO<sub>3</sub> films for memory applications. *Appl. Phys. Lett.* **87**, 102903 (2005)
63. J.F. Ihlefeld, N.J. Podraza, Z.K. Liu, R.C. Rai, X. Xu, T. Heeg, Y.B. Chen, J. Li, R.W. Collins, J.L. Musfeldt, X.Q. Pan, J. Schubert, R. Ramesh, D.G. Schlom, Optical band gap of BiFeO<sub>3</sub> grown by molecular-beam epitaxy. *Appl. Phys. Lett.* **92**, 142908 (2008)
64. P.S.V. Mocherla, C. Karthik, R. Ubic, M.S. Ramachandra Rao, C. Sudakar, Tunable band gap in BiFeO<sub>3</sub> nanoparticles, the role of microstrain and oxygen defects. *Appl. Phys. Lett.* **103**, 022910 (2013)
65. R.R. Das, D.M. Kim, S.H. Baek, C.B. Eom, F. Zavaliche, S.Y. Yang, R. Ramesh, Y.B. Chen, X.Q. Pan, X. Ke, M.S. Rzchowski, S.K. Streiffner, Synthesis and ferroelectric properties of epitaxial BiFeO<sub>3</sub> thin films grown by sputtering. *Appl. Phys. Lett.* **88**, 242904 (2006)
66. Y. Wang, Q. Jiang, H. He, C.-W. Nan, Multiferroic BiFeO<sub>3</sub> thin films prepared via a simple sol-gel method. *Appl. Phys. Lett.* **88**, 142503 (2006)
67. J. Wang, Y. Wei, J. Zhang, L. Ji, Y. Huang, Z. Chen, Synthesis of pure-phase BiFeO<sub>3</sub> nanopowder by nitric acid-assisted gel. *Mater. Lett.* **124**, 242–244 (2014)
68. S.K. Singh, R. Ueno, H. Funakubo, H. Uchida, S. Koda, H. Ishiwara, Dependence of ferroelectric properties on thickness of BiFeO<sub>3</sub> thin films fabricated by chemical solution deposition. *Jpn. J. Appl. Phys.* **44**, 12 (2005)
69. A. Huang, S.R. Shannigrahi, Effect of bottom electrode and resistive layer on the dielectric and ferroelectric properties of sol-gel derived BiFeO<sub>3</sub> thin films. *J. Alloys Compd.* **509**, 2054–2059 (2011)
70. S. Sharma, P. Saravanan, O.P. Pandey, V.T.P. Vinod, M. Cernik, P. Sharma, Magnetic behaviour of sol-gel driven BiFeO<sub>3</sub> thin films with different grain size distribution. *J. Magn. Mater.* **401**, 180–187 (2016)
71. S. Zheng, J. Wang, J. Zhang, H. Ge, Z. Chen, Y.F. Gao, The structure and magnetic properties of pure single phase BiFeO<sub>3</sub> nanoparticles by microwave-assisted sol-gel method. *J. Alloys Compd.* **735**, 945–949 (2018)
72. H. Wu, P. Xue, Y. Lu, X. Zhu, Microstructural, optical and magnetic characterizations of BiFeO<sub>3</sub> multiferroic nanoparticles synthesized via a sol-gel process. *J. Alloys Compd.* **731**, 471–477 (2018)
73. S. Iakovlev, C.-H. Solterbeck, M. Kuhnke, M. Es-Sounia, Multiferroic BiFeO<sub>3</sub> thin films processed via chemical solution deposition: structural and electrical characterization. *J. Appl. Phys.* **97**, 094901 (2005)
74. P. Khare, S. Talebi, B. Ramachandran, A. Dixit, V.M. Naik, M.B. Sahana, C. Sudakar, R. Naik, M.S.R. Rao, G. Lawes, Structural, magnetic, and electrical studies on polycrystalline transition-metal-doped BiFeO<sub>3</sub> thin films. *J. Phys. Condens. Matter.* **21**, 036001 (2009)
75. S.K. Singha, H. Ishiwara, Enhanced polarization and reduced leakage current in BiFeO<sub>3</sub> thin films fabricated by chemical solution deposition. *J. Appl. Phys.* **100**, 064102 (2006)
76. S.W. Chen, J.M. Wu, Unipolar resistive switching behaviour of BiFeO<sub>3</sub> thin films prepared by chemical solution deposition. *Thin Solid Films* **519**, 499–504 (2010)
77. Y. Wang, Y. Lin, C.-W. Nan, Thickness dependent size effect of BiFeO<sub>3</sub> films grown on LaNiO<sub>3</sub>-buffered Si substrates. *J. Appl. Phys.* **104**, 123912 (2008)

78. X. Chena, H. Zhang, K. Ruan, W. Shi, Annealing effect on the bipolar resistive switching behaviours of BiFeO<sub>3</sub> thin films on LaNiO<sub>3</sub>-buffered Si substrates. *J. Alloys Compd.* **529**, 108–112 (2012)
79. A.J. Hatt, N.A. Spaldin, Strain-induced isosymmetric phase transition in BiFeO<sub>3</sub>. *Phys. Rev. B* **81**, 054109 (2010)
80. S.V. Trukhanov, I.O. Troyanchuk, I.M. Fita, H. Szymczak, K. Bärner, Comparative study of the magnetic and electrical properties of Pr<sub>1-x</sub>Ba<sub>x</sub>MnO<sub>3-δ</sub> manganites depending on the preparation conditions. *J. Magn. Magn. Mater.* **237**, 276–282 (2001)
81. S.V. Trukhanov, L.S. Lobanovski, M.V. Bushinsky, I.O. Troyanchuk, H. Szymczak, Magnetic phase transitions in the anion-deficient La<sub>1-x</sub>Ba<sub>x</sub>MnO<sub>3-x/2</sub> (0 ≤ x ≤ 0.50) manganites. *J. Phys. Condens. Matter.* **15**, 1783–1795 (2003)
82. S.V. Trukhanov, A.V. Trukhanov, H. Szymczak, C.E. Botez, A. Adair, Magnetotransport properties and mechanism of the A-site ordering in the Nd–Ba optimal-doped manganites. *J. Low Temp. Phys.* **149**, 185–199 (2007)
83. T.J. Park, G.C. Papaefthymiou, A.J. Viescas, A.R. Moodenbaugh, S.S. Wong, Size-dependant magnetic properties of single-crystalline multiferroic BiFeO<sub>3</sub> nanoparticles. *Nano Lett.* **7**, 766–772 (2007)
84. J. Santoyo-Salazar, M.A. Castellanos-Roman, L. Beatriz, Gómez, Structural and magnetic domains characterization of magnetite nanoparticles. *Mater. Sci. Eng. C* **27**, 1317–1320 (2007)
85. S.V. Trukhanov, A.V. Trukhanov, A.N. Vasiliev, H. Szymczak, Frustrated exchange interactions formation at low temperatures and high hydrostatic pressures in La<sub>0.70</sub>Sr<sub>0.30</sub>MnO<sub>2.85</sub>. *JETP* **111**, 209–214 (2010)
86. S.V. Trukhanov, A.V. Trukhanov, A.N. Vasiliev, A.M. Balagurov, H. Szymczak, Magnetic state of the structural separated anion-deficient La<sub>0.70</sub>Sr<sub>0.30</sub>MnO<sub>2.85</sub> manganite. *JETP* **113**, 819–825 (2011)
87. C.J. Cheng, C. Lu, Z. Chen, L. You, L. Chen, J. Wang, T. Wu, Thickness-dependent magnetism and spin-glass behaviors in compressively strained BiFeO<sub>3</sub> thin films. *Appl. Phys. Lett.* **98**, 242502 (2011)
88. F. Huang, Z. Wang, X. Lu, J. Zhang, K. Min, W. Lin, R. Ti, T.T. Xu, J. He, C. Yue, Z. Zhu, Peculiar magnetism of nanoparticles with size approaching the period of the spiral spin structure. *Sci. Rep.* **3**, 2907 (2013)
89. R. Gupta, S. Chaudhary, R.K. Kotnala, Interfacial charge induced magnetoelectric coupling at BiFeO<sub>3</sub>/BaTiO<sub>3</sub> bilayer interface. *ACS Appl. Mater. Interfaces* **7**, 8472–8479 (2015)

**Publisher's Note** Springer Nature remains neutral with regard to jurisdictional claims in published maps and institutional affiliations.